Semicond. Sci. Technol. **26** (2011) 075011 (6pp) doi:10.1088/0268-1242/26/7/075011

# Diode ideality factor in modern light-emitting diodes

**Hisashi Masui**

Weekend Optoelectronics Wonderland, 56 South Patterson Avenue, Santa Barbara, CA 93111, USA

E-mail: masui@alumni.engr.ucsb.edu

Received 30 January 2011, in final form 30 January 2011
Published 11 April 2011
Online at stacks.iop.org/SST/26/075011

**Abstract**

The diode ideality factor has been subjected to theoretical discussions from the viewpoint of light-emitting diodes (LEDs). As radiative recombination in LEDs is incongruent with the Sah–Noyce–Shockley (SNS) analysis, the SNS recombination plane was replaced with carrier confinement structures of modern LEDs, e.g., quantum wells (QWs). We calculated the voltage partitioning factors to indicate how carrier concentration changes as a function of terminal voltage. As local minority carriers determine the net recombination rate at QWs, we have deduced that the partitioning factor of the local minority carriers becomes the ideality factor of the LED. By applying incomplete ionization of acceptors in InGaN/GaN LEDs, a conclusion has been reached such that the partitioning factor of local minority carriers as well as the diode ideality factor can be nearly as large as 3.

(Some figures in this article are in colour only in the electronic version)

## 1. Introduction

The current–voltage ($I$–$V$) relationship is a fundamental property of the diode. Current depends on voltage exponentially due to the fact that the carrier distribution in energy is exponential under the Boltzmann approximation. The $I$–$V$ relationship is expressed by the diode equation

$$I = I_S\{\exp[qV/(nkT)] - 1\}, \tag{1}$$

where $I$ is the diode current, $I_S$ is the reverse saturation current, $q$ is the unit charge, $V$ is the terminal voltage, $k$ is the Boltzmann constant, and $T$ is the absolute temperature. The fudge factor $n$ is called the diode ideality factor. The Sah–Noyce–Shockley (SNS) analysis gave a physical meaning to the ideality factor [1, 2]; $n = 2$ has been assigned for the recombination current, which is defined as due to recombination in the depletion layer. The SNS analysis was carried out on a Si diode that is an indirect band gap material and radiation was improbable as a result of recombination. The light-emitting diode (LED) became a subject of extensive research and practical use after the SNS analysis was established. The same notion of the recombination current has been implicitly applied to LEDs without careful inspection, however. LEDs utilize direct band gap materials and radiation is expected. Indeed, recombination in the depletion layer is the central mechanism of the LED. In modern LEDs, we use carrier confinement heterostructures by virtue of epitaxial techniques rather than diffusion techniques. Carrier confinement structures are understood to be the efforts to minimize the injection current ($n = 1$), which is defined as due to recombination outside the depletion layer.

The awkwardness of applying the SNS analysis to LEDs was recognized explicitly when III-nitride LEDs emerged. III-nitride LEDs have high operation voltage compared to emitted photon energy, and the ideality factor is part of the reason. It has been a common observation that the ideality factor appears to be greater than 2, reaching up to 7, which is inconsistent with the conclusion of the SNS analysis. Several reports attributed the large values to the tunneling current, often via deep levels. Fadison *et al* presented a thorough discussion on the tunneling current in a GaN pn junction [3]. The proposed paths of the recombination–tunneling process are unlikely to generate photons with band gap energy. Generally, evidence of deep levels is rarely observed in electroluminescence. One answer was given by Shah *et al*, who proposed a theoretical model for the large ideality factors by taking into account the multiple junctions within a device [4]. Their theory did not address the meaning of the SNS ideality factor and left it as it was given, adopting trap levels in the band gap. These past studies discussed the large ideality factors under the assumption that the ideality factor did not exceed 2 based on the SNS analysis, despite

 

the fact that the SNS analysis did not account for band-to-band recombination. Acharya *et al* mentioned that the ideality factor could be up to 3, but mysteriously, details were not discussed [5].

As there has been no attempt to interpret the SNS analysis from the viewpoint of LEDs, this study explores how $n > 2$ is feasible in III-nitride LEDs by contrasting the notions introduced in the SNS analysis.

## 2. Analysis and discussions

### 2.1. Role of the recombination plane in the SNS analysis

The SNS analysis made the advancement based on the notion of the recombination plane. According to [1], the net recombination rate $U_{\mathrm{SNS}}$ is expressed as

$$U_{\mathrm{SNS}} = \left(pn - n_i^2\right)/[(n+n_1)\tau_{p0} + (p+p_1)\tau_{n0}] \qquad (2)$$

(reproduction of equation (6) of [1]). Equation (2) tells us that when trap levels are near the mid gap (hence, $n_1 \sim p_1$) and lifetimes of electrons and holes at the trap levels are similar ($\tau_{n0} \sim \tau_{p0}$), $U_{\mathrm{SNS}}$ becomes high at the position $x$ where electron concentration $n = n(x)$ and hole concentration $p = p(x)$ are comparable. Thus, the requirement of equation (2) is $n(x) \approx p(x)$, which defines the recombination plane near the intrinsic point (where $n(x) = p(x)$) in the three-dimensional bar of material. (NB The ideality factor $n$ should not be confused with the electron concentration $n$.) This means $n(x)$ and $p(x)$ always need to increase equally when $V$ is increased; in order to achieve that, half of $V$ (i.e. $n = 2$) is spent for each type of carriers. As the recombination rate is the current, under the Shockley–Read–Hall (SRH) conditions, $n = 2$ for the recombination current is a rigid conclusion regardless of the doping symmetry of the junction. The recombination plane moves with $V$ in asymmetrically doped junctions to seek for the point where $n \approx p$ [6]. The SRH statistics tells that traps at or near the middle of the band gap are the most active in assisting recombination [7, 8], so that the requirement $n \approx p$ is for the recombination plane.

The material quality of III–V semiconductors has been improved such that stimulated emission can be obtained; thus, band-to-band emission is possible with high quantum efficiencies. As we do not observe trap-level-related electroluminescence, trap levels are believed to be barely existent in LED active regions. High recombination rates occur because of the carrier confinement structures of modern LEDs, which can then be considered to be highly efficient recombination centers and replace the SNS recombination plane in the theoretical analysis. With this concept, the following analysis does not depend on the SRH statistics or equation (2). For band-to-band recombination, the recombination rate is proportional to the product of carrier concentrations. We therefore wish to explore carrier concentration in the depletion layer explicitly as a function of $x$ and $V$.

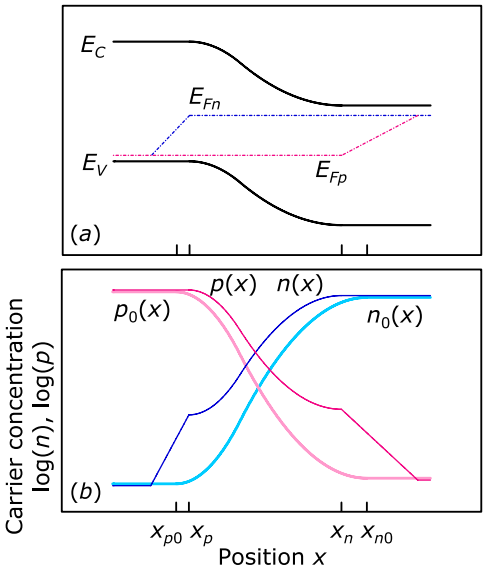


**Figure 1.** (*a*) Band diagram of a pn homo junction under positive bias. Quasi Fermi levels $E_{Fn}$ and $E_{Fp}$ have been drawn under the condition where no recombination takes place in the depletion layer. (*b*) Carrier concentration profiles $n(x)$ and $p(x)$ (on a logarithmic scale) corresponding to (*a*) along with equilibrium ones $n_0(x)$ and $p_0(x)$. This particular example has been drawn for $N_A$:$N_D$ = 1:2 ($N_A$ and $N_D$ are acceptor and donor concentrations, respectively).

### 2.2. Carrier concentration as a function of V

Let us consider a homo junction under positive bias with no net recombination in the depletion layer (figure 1). Quasi Fermi levels remain flat across the depletion layer. Carrier concentration can be calculated via the Boltzmann approximation. $n(x)$ and $p(x)$ change accordingly by reflecting contraction of the depletion layer and reduction of the built-in potential. Electron concentration $n(x, V)$ is

$$n(x, V) = N_C \exp\left[\frac{(E_C(x, V) - E_{Fn}(x, V))}{kT}\right], \qquad (3)$$

where $N_C$ is the effective density of states at the conduction band edge $E_C$. The quasi Fermi level for electrons, $E_{Fn}$, has been taken to be the reference potential. Hole concentration $p(x,V)$ is determined similarly. Going into the opposite side of the junction, injected carrier concentration dies out exponentially, which is the source of the injection current. Here, the key parameter is $E_C(x, V) - E_{Fn}(x, V)$ and $E_{Fp}(x, V) - E_V(x, V)$ ($E_{Fp}$ is the quasi Fermi level for holes and $E_V$ is the valence band edge). These terms need to be written explicitly in terms of $V$.

It is convenient to introduce the notion of the voltage partitioning factor to understand how applied voltage generates excess carriers. $E_C$ under positive bias has been drawn in figure 2 in two distinctive ways. With respect to the black curve $\left(E_C^0(x)\right)$ representing $E_C$ at equilibrium, the blue curve $\left(E_C^b(x)\right)$ indicates $E_C$ under positive bias $V$ keeping the potential of the n-type neutral region constant. The electrostatic potential at the edge of the depletion layer on the p-type side ($x_p$), $E_C(x_p)$, changes as $V/1$; thus, the p-type neutral region receives the full applied voltage. The potential of the n-type neutral region is always zero. In between, $E_C$

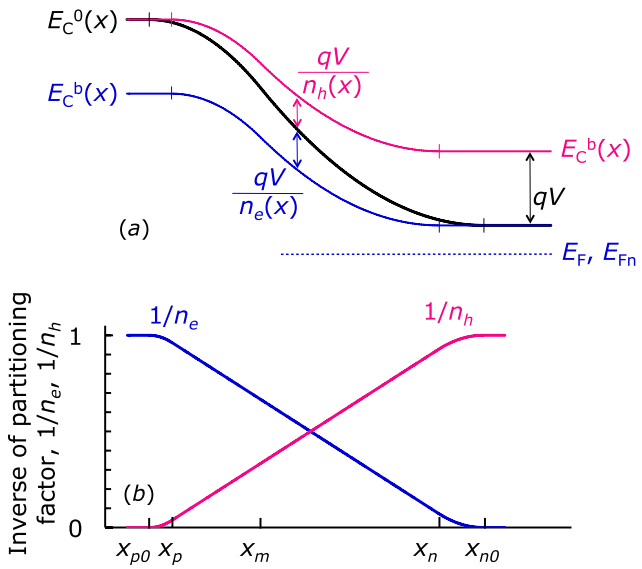


**Figure 2.** (*a*) Two ways of presenting $E_C$ under positive bias, $E_C^b(x)$, with respect to $E_C$ at equilibrium, $E_C^0(x)$. (*b*) Corresponding partitioning factors $n_e$ and $n_h$ plotted as their inverse.

receives a part of $V$ and it is a function of $x$. We write the voltage partitioning as $V/n_e(x)$. The red curve is also $E_C^b(x)$ but is drawn for the p-type neutral region maintaining the constant potential.[1] Partitioning factors for electrons and holes, $n_e(x)$ and $n_h(x)$, indicate how much of $V$ is partitioned to blue (for electrons) and red (for holes) curves at $x$. Calculated partitioning factors (the method of calculation is shown in the next paragraph) are plotted in figure 2(*b*) as their inverse. They change monotonically over the depletion layer and the slopes of the line excluding the edges are constant. The difference between the two $E_C^b(x)$ curves is $qV$ and not a function of $x$; hence, the two partitioning factors are complementary:

$$\frac{1}{n_e(x)} + \frac{1}{n_h(x)} = 1. \tag{4}$$

One thing to note is that an approximation has been made such that $E_{Fn}$ is stationary with respect to $E_C$ in the neutral region, implying that $V$ is not too large. With equation (3), electron concentration at $x$ is

$$n(x, V) = n_0(x) \exp\left[\left(E_C^b(x) - E_C^0(x)/(kT)\right]\right. \tag{5}$$

$$= n_0(x) \exp[qV/(n_e kT)], \tag{6}$$

where $n_0(x)$ is the equilibrium electron concentration at $x$. The blue arrow in figure 2 assists to deduce equation (6). Similarly, hole concentration is $p(x, V) = p_0(x) \exp[qV/(n_h(x)kT)]$.

The method to calculate the voltage partitioning factor at an arbitrary $x$ is as follows. Figure 3 illustrates the electric field distribution in the depletion layer. The applied voltage corresponds to the shaded area being equal to $qV$. The electrostatic potential at $x$ is obtained by integrating the field

[1] It may be intuitively done with $E_V$ for holes; nevertheless, the argument is fundamentally equivalent.

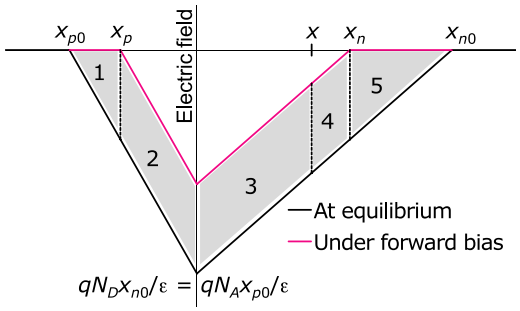


**Figure 3.** Method to calculate the electrostatic potential at $x$. The electric field is shown as a function of position under equilibrium (black) and positive bias (red) conditions. The area under the curve corresponds to the electrostatic potential. The area has been divided into five subareas for the sake of convenience.

curve from either side, depending on which side is taken to be the ground. Voltage partitioning at $x$ is determined by the ratio of the shaded area between the right and left sides with respect to $x$. In figure 3, the shaded area has been divided into five subareas. The subarea 1 is

$$\frac{qN_A}{2\epsilon}(x_p - x_{p0})^2, \tag{7}$$

where $N_A$ is the acceptor concentration, $\epsilon$ is the dielectric constant of the material, and $x_{p0}$ is the depletion layer edge on the p-type side at equilibrium. The other four subareas are formalized similarly. According to the junction theory,

$$x_p - x_n = \sqrt{\frac{2\epsilon}{q}\frac{N_A + N_D}{N_A N_D}(V_{bi0} - V)} \tag{8}$$

($x_n$ is the edge of the depletion layer on the n-type side, $N_D$ is the donor concentration, $V_{bi0}$ is the built-in voltage at equilibrium) and

$$x_p : x_n = x_{p0} : x_{n0} = N_D : N_A \tag{9}$$

($x_{n0}$ is the depletion layer edge on the n-type side at equilibrium). From equations (8) and (9),

$$x_p - x_{p0} = \sqrt{\frac{2\epsilon}{q}\frac{1}{N_A + N_D}\frac{N_D}{N_A}}(\sqrt{V_{bi0}} - \sqrt{V_{bi0} - V}) \tag{10}$$

that is plugged back into equation (7). A similar equation can be obtained for the n-type side, $x_{n0} - x_n$. The partitioning factors at $x$ are obtained as a ratio between the partial area and the entire shaded area.

### *2.3. Recombination rate as a function of carrier concentration*

Quantum wells (QWs) can be regarded as efficient recombination centers, as the concept has been proposed in our previous publication [9]. Let us now find how the recombination rate changes when $V$ is changed. The net recombination rate $U_0$ can be written as

$$U_0 = B\left(n(x)p(x) - n_i^2\right) \tag{11}$$

$$= B(n_0(x)p_{ex}(x) + p_0(x)n_{ex}(x) + n_{ex}(x)p_{ex}(x)) \tag{12}$$

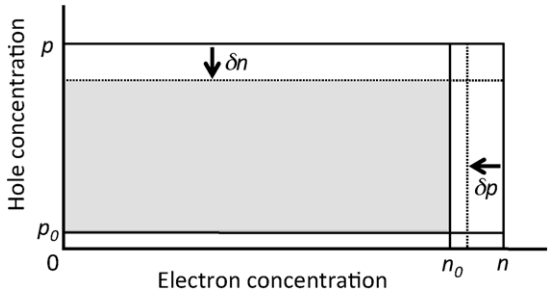


**Figure 4.** Visual representation of the recombination rate at an arbitrary $x$ (chosen in the n-type side of the junction) and positive $V$. $\delta n$ and $\delta p$ are reduction in carrier concentration due to net recombination. The shaded area is $n_0(p_{ex} - \delta)$.

($n_{ex}$ and $p_{ex}$ are excess electron and hole concentrations, $n_i$ is the intrinsic carrier concentration, and $B$ is a proportionality constant). From this, one can immediately deduce that recombination is promoted at carrier confinement regions (i.e. QWs) regardless of $x$. At QWs, $n_0$ and $p_0$ are large because $n_i$ is larger for a smaller band gap. Additionally, from equation (6), the larger the equilibrium carrier concentration, the larger is the excess carrier concentration. As a consequence of net recombination, quasi Fermi levels are no longer flat across the QWs (see appendix A).

It is a common understanding that excess minority carrier concentration determines the net recombination rate. In our case, $n(x, V)$ and $p(x, V)$ have been given under the condition of no net recombination (equation (6)). Figure 4 is to show visually that excess minority carrier concentration dominates net recombination by taking into account that recombination consumes both types of carriers equally. As the recombination rate is proportional to the product of both carrier concentrations, the rectangle areas in figure 4 represent the contribution to the recombination rate. The largest rectangle represents $n(x, V)p(x, V)$. The rectangle of $n_0$ by $p_0$ is equal to $n_i^2$, which corresponds to the equilibrium carrier generation rate. By net recombination, part of excess carriers, $\delta n$ and $\delta p$, annihilate due to the fact that the carrier supply rate is finite. The resulting rectangle (surrounded by the broken lines) is proportional to the net recombination rate under the steady state condition, $U_1$. At $x$ in the n-type side of the depletion layer,

$$U_1 = B\left[(p - \delta p)(n - \delta n) - n_i^2\right] \tag{13}$$

$$= B[p_0(n_{ex} - \delta n) + n_0(p_{ex} - \delta p) + (p_{ex} - \delta p)(n_{ex} - \delta n)] \tag{14}$$

$$\sim B[n_0(p_{ex} - \delta)], \tag{15}$$

where $\delta n = \delta p \equiv \delta$ has been implemented. The second term in equation (14) dominates, as can be confirmed via figure 4 (shaded area). $p_{ex} = p - p_0$ is large because of the small partitioning factor of holes. $n_0$ and $p_0$ can be different by many orders of magnitude. Thus, net recombination is dominated by the local excess minority carriers. It can be shown rigorously that local minority carriers always have a partitioning factor less than 2 (figures 1 and 2). The ideality factor then never exceeds 2.

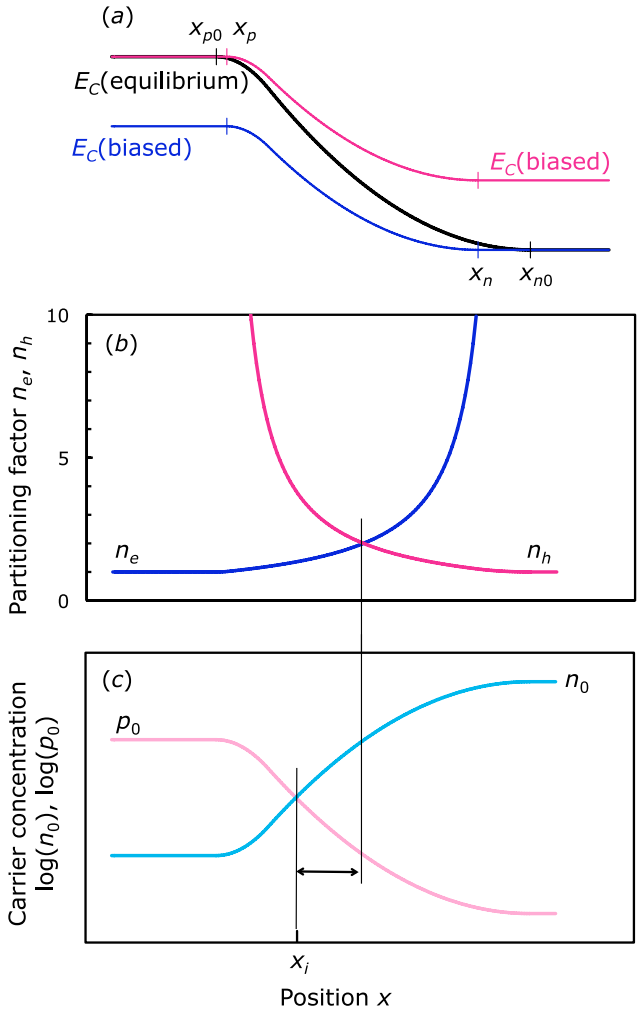


**Figure 5.** Showing the skewed situation for $N_A$:$N_D$ = 5:1. (*a*) $E_C$ represented in the same way as figure 2(*a*). (*b*) Partitioning factors calculated via electrostatic potential of the junction. (*c*) Carrier concentration profiles under incomplete ionization of acceptors. $x_i$ is the intrinsic point. The arrow indicates the region where the local minority carrier has a partitioning factor greater than two.

Another method of calculating the net recombination rate is given in appendix B.

### *2.4. Skewed situation of the III-nitride pn junction*

A common donor for III-nitride materials is Si and $10^{17}$–$10^{18}$ cm$^{-3}$ is a typical range for doping concentration. Mg is a common acceptor, which tends to be doped much more heavily ($10^{19}$–$10^{20}$ cm$^{-3}$) because of ∼1% of thermal ionization at ambient temperature. As a result, the pn junction becomes extremely asymmetric. The resulting skewed situation ($N_A > N_D$ but $p_0(x_{p0}) < n_0(x_{n0})$) gives rise to a significant departure from fully-ionized cases. The effects of the skewed situation may become clearer via figure 5, where $E_C$ of an asymmetric junction has been drawn in the same way as figure 2(*a*) along with partitioning factors and equilibrium carrier concentration. The intrinsic point

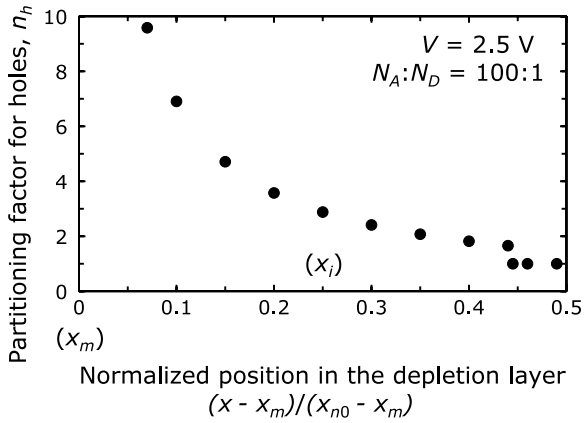


**Figure 6.** $n_h$ as a function of $x$. $x_m$ is the position of the metallurgical junction and $x_m \approx x_p$ in this example. The abscissa indicates the distance from $x_m$ toward the n-type side and beyond 0.25 (the intrinsic point $x_i$) is where holes are minority carriers. Beyond 0.44, $n_h(x) = 1$ because $x > x_n$.

is closer to $x_p$ than $x_n$ and the hole partitioning factor is large near the p-type neutral region. As a result, holes as minority carriers have a partitioning factor greater than 2 in the region of $x$ shown by an arrow in figure 5(*c*). If a QW is placed in this region, the ideality factor becomes greater than 2 due to the fact that the recombination rate (i.e. current) varies with local excess minority carrier concentration. This finding explains our previous experimental observations of $n > 2$ [9].

To perform a numerical calculation, a typical GaN pn junction is considered. Parameters are $N_A = 5 \times 10^{19}$ cm$^{-3}$, $N_D = 5 \times 10^{17}$ cm$^{-3}$, and $V_{bi0}$ was taken to be 3.2 V. For these doping concentrations, the depletion layer barely extends into the p-type layer and the band bending is almost simply quadratic. Carrier concentration profiles (on a logarithmic scale) are then also quadratic. If 1% of thermal acceptor ionization is applicable, $n_0(x_{n0}) = p_0(x_{p0})$. The intrinsic point happens at $(1/2)^2(x_{n0} - x_{p0})$: a quarter of the depletion layer thickness from the metallurgical junction toward the n-type side. Figure 6 plots $n_h(x)$ as a function of $x$ for $V = 2.5$ V. Holes are minority carriers beyond 0.25 and there is a range of $x$ where $n_h > 2$; hence, the minority carrier can have a partitioning factor greater than 2 under skewed situations.

As for the quantum-confined Stark effect (QCSE), even though it has tremendous effects on InGaN QW performances, it plays only a minimal role in the ideality factor discussion within the conditions that the QW is sufficiently thin compared with the depletion layer. This is because the area under the electric field curve is negligible under such conditions.

## 3. Conclusion

The theoretical analysis of the diode ideality factor was performed from the viewpoint of LEDs. The SNS recombination plane was discarded due to the fact that electroluminescence was scarcely related to trap levels, and replaced with the carrier confinement structure of modern LEDs. The partitioning factors were introduced to relate carrier concentration in the depletion layer to the applied voltage. The net recombination rate was shown to be dominated by local minority carriers, which always have partitioning factors smaller than two under fully-ionized impurity conditions. By applying the skewed situation of pn junctions commonly found in III-nitride LEDs, we have reached the conclusion that the partitioning factor of local minority carriers can be as large as approximately 3, and the ideality factor can thus be as large as approximately 3.

## Appendix A. Quasi Fermi levels in the depletion layer

It is often stated that $E_{Fn} - E_{Fp} \approx qV$ and the recombination rate is written as

$$U_0 = B(x)\left(n(x)p(x) - n_i^2\right) \tag{A.1}$$

$$= B(x)n_i^2\left[\exp\left(\frac{E_{Fn}(x) - E_{Fp}(x)}{kT}\right) - 1\right]. \tag{A.2}$$

Since equation (A.2) does not involve the ideality factor, it may seem in conflict with equation (1). The statement in fact needs to be more accurate: $E_{Fn}(x_n) - E_{Fp}(x_p) \approx qV$. Equation (1) is then written as

$$I \approx I_S\left[\exp\left(\frac{E_{Fn}(x_n) - E_{Fp}(x_p)}{nkT}\right) - 1\right]. \tag{A.3}$$

$E_{Fn}(x) - E_{Fp}(x) \neq qV$ when recombination is happening at $x$, while the quasi Fermi level separation at the edges of the depletion layer remains the same. In equation (A.2), the carrier confinement effect has been absorbed into $n_i(x)$, whereas the effect is described by $n$ in equation (A.3).

It is impractical to determine quasi Fermi level profiles accurately in a pn junction. Quasi Fermi levels can be determined uniquely only when the space distribution of the recombination rate is specified. To do so, it is essential to treat $B$ as a function of $x$. In addition, equation (A.2) requires careful consideration when the band gap is a function of $x$ (i.e. heterostructures). Electron concentration is determined by $E_C(x) - E_{Fn}(x)$, which may not be a smooth and monotonic function of $x$; the same argument applies for hole concentration. The effective density of states can be a function of $x$ as well, but it is usually less influential than the exponential term in the Boltzmann function.

The primitive junction analysis often assumes that recombination in the depletion layer is negligible for the reason that the built-in field sweeps carriers rapidly into the neutral regions. That is, $B(x_p < x < x_n) \approx 0$ and $B(x < x_p)$ and $B(x_n < x)$ are finite (e.g., figure 2). This profile of $B(x)$ results in a truly unity ideality factor. The SNS analysis

reached $B(x_p < x < x_n) \neq 0$. In the present analysis, $B$ is finite across the depletion layer.

## Appendix B. Analytical method of calculating the recombination rate

Carrier consumption by net recombination is proportional to the net recombination rate, $\delta = \beta U_1$, where the proportionality constant $\beta$ has units of time:

$$U_1 = B\left[(n - \delta n)(p - \delta p) - n_i^2\right] \tag{B.1}$$

$$= B\left[np - \beta(n + p)U_1 + \beta^2 U_1^2 - n_i^2\right]. \tag{B.2}$$

This is a quadratic equation in terms of $U_1$, $\beta^2 U_1^2 - [(n+p)\beta + (1/B)]U_1 + np - n_i^2 = 0$, which can be readily evaluated when $\beta$ is small (i.e. $\beta^2 \sim 0$):

$$U_1 = \left(np - n_i^2\right)/[(n + p)\beta + (1/B)]. \tag{B.3}$$

The numerator is analytically precisely proportional to $\exp[qV/(kT)]$. For $n > p$, the denominator is approximately proportional to $n$, which is proportional to $\exp[qV/(n_e kT)]$. Hence,

$$U_1 \propto \exp[qV/(kT)]/\exp[qV/(n_e kT)] \tag{B.4}$$

$$= \exp[qV/(n_h kT)], \tag{B.5}$$

where equation (4) has been used. The ideality factor appears close to $n_h$, and becomes near unity for high injection and high recombination. Such a trend was confirmed in our previous study [9].

## References


[1] Sah C T, Noyce R N and Shockley W 1957 *Proc. IRE* **45** 1228
[2] Sah C T 1991 *Fundamentals of Solid-State Electronics* (Singapore: World Scientific) pp 432–41
[3] Fadison J B, Chow T P, Lu H and Bhat I B 1998 *Appl. Phys. Lett.* **72** 2841
[4] Shah J M, Li Y-L, Gessmann Th and Schubert E F 2003 *J. Appl. Phys.* **94** 2627
[5] Acharya Y B and Vyavahare P D 1999 *Solid-State Electron.* **43** 645
[6] Mishra U K and Singh J 2008 *Semiconductor Device Physics and Design* (Dordrecht: Springer) chapter 4
[7] Shockley W and Read W T Jr 1952 *Phys. Rev.* **87** 835
[8] Hall R N 1952 *Phys. Rev.* **87** 387
[9] Masui H, Nakamura S and DenBaars S P 2010 *Appl. Phys. Lett.* **96** 073509